International Journal of Advanced Engineering and Management Research

Vol. 6, No. 06; 2021

ISSN: 2456-3676

UNFOLDING OF GAMMA RAY AND ELECTRON SPECTRA OF A PLASTIC SCINTILLATOR AT AIRCRAFT FLIGHT ALTITUDES

Sadia Assad[1], Adam Skorek[1], Fidele Moupfouma[1]
[1]Department of Electrical and Computer Engineering, University of Quebec,
Trois Rivières, Quebec, Canada

Abstract
Today, aircraft flights are carried out over very long distances and at very high altitudes. However, at very high altitudes and at higher or lower latitudes, the environmental threat associated with cosmic radiation becomes more acute and therefore the risks to equipment become greater.

In order to assess the impact of cosmic rays on systems during aircraft flights and therefore the risks for aircraft safety, it then becomes necessary to quantify the presence of these cosmic rays and their effects at high flight altitudes of aircraft.

To this end, Bombardier Aerospace and its partners have launched measurement campaigns on board aircraft flying at different latitudes at high altitudes. A plastic scintillator has been used to measure cosmic ray particles to build up a consistent database of real data. However, the measurements recorded by this scintillator must be converted into spectra, which can be used to assess the effects of cosmic radiation on electronic modules. Thus, for the work exposed in this paper, we have selected and used the Gravel algorithm to transform the measured data into gamma rays and electrons spectrum energy.

The accuracy of the energy fluence for many points of the flight path is assessed by comparing the effective dose calculations from the measurements and those using the following tool: based on excel programs for the calculation of atmospheric cosmic ray spectrum (EXPACS). The rate differences between these doses for altitudes above 6 km do not exceed 19%, these ones are acceptable in spectroscopy.

Keywords: Aircraft; Gamma rays; Electrons; Measurements; Gravel algorithm; MCNP6

1. Introduction

Cosmic rays can interact with matter and, to do so, they have a high penetrating power. This is why they can constitute a real threat for semiconductors, both by their size and by the material in which they are made, such as silicon. This resulting ionized material can trigger a single event upset (SEU) on the integrated system on board the aircraft [1].

For more than three decades, the aerospace industry has favored reducing the weight of aircraft, by reducing fuel consumption during flights, while promoting increasingly long flights at high altitude. The miniaturization of electronic components, in particular integrated circuits, also contributes to the achievement of this objective.

Vol. 6, No. 06; 2021

ISSN: 2456-3676

At aircraft flight altitudes, the particle energetic fluence rate takes into account variations in particle fluence rates arising from galactic cosmic radiation (GCR) and solar energetic particles (SEP). The first compound is regular and depends on the solar cycle, geomagnetic coordinates and atmospheric thickness. However, the second compound is spontaneous and depends on random solar flares and coronal mass ejection [2-3].

Both GCR and SEP particles can reach the upper part of the Earth's atmosphere with an average energy of 106 MeV and 103 MeV respectively [4]. But their energies are reduced proportionally before reaching the ground, by the multi-interactions between these particles with air molecules such as nitrogen and oxygen as shown in Figure 1.

However, at very high flight altitudes of airplanes, gamma rays and neutrons are the main threat from cosmic rays and, this risk is overcome by an accurate assessment of the immunity of the semiconductor device against the cosmic rays available at these altitudes. Therefore, in order to define the appropriate mitigation parameters, an assessment of this resulting risk requires that the calculations of the fluence rates necessary for the design of the device and the commissioning of this device are integrated into the estimation systems of error rates [5].

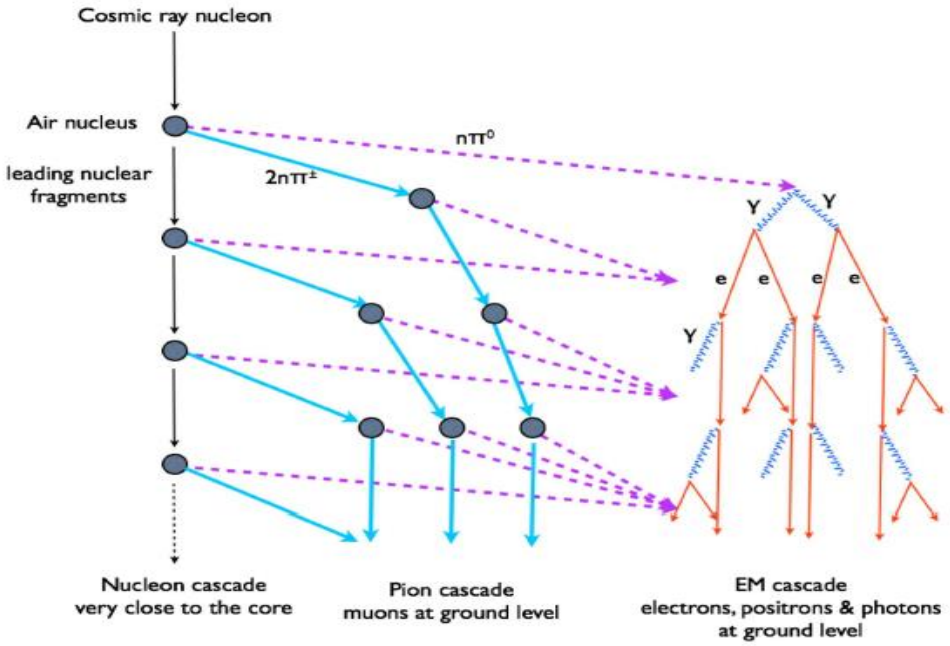

Figure 1. Disintegration of a primary cosmic ray in contact with the atmosphere [6]

In this context, Bombardier with the support of some academic and industrial partners carried out a campaign to measure the impact of cosmic radiations on the safety of aircraft flights. As such, an EJ299-33A plastic scintillator has been used as part of the setup on board the Global 7500 test aircraft. The choice of this plastic scintillator is governed by its robustness and mainly by its

Vol. 6, No. 06; 2021

ISSN: 2456-3676

good capacity to discriminate between neutrons and gamma rays in the mixed field of cosmic radiation [7].

However, due to the intrinsic specifications of plastic scintillators which give them such low energy resolution, low density and low light output, plastic scintillators do not have good characteristics for measuring gamma rays [8-11]. Thus, unlike inorganic scintillators such as NaI: TI (sodium iodide activated with thallium) and semiconductor detectors such as HPGe (high purity germanium), the plastic scintillator does not make it possible to obtain the full energy peak [12]. In the other hand, these other detectors cited above don't have good features for the discrimination. In addition, these detectors could deteriorate on contact with high energies and also promote an increase in temperature variations.

On the other hand, the predominant interaction of gamma rays in the active volume of the plastic scintillator is Compton scattering [13]. Moreover, the mixed field of cosmic radiation at aircraft flight altitudes contains fast electrons, which could also strike the scintillator material, and precisely the plastic scintillator has good characteristics for detecting and measuring fast electrons, due to its low atomic number. Thus, the PHS (pulse height spectrum) recorded from the experimental platform is proportional to the energy deposited in the scintillator by the electron, generated jointly by the gamma ray and the incident fast electron.

It is in this context that the unfolding of the measured spectra is required to obtain the spectra of the desired incident particles, necessary to develop the appropriate studies [14]. For this reason, the unfolding process involves the computation of the scintillator response function, using software based on the Monte Carlo method (MCNP6) in this article [15]. Then, the introduction of the energy response functions and the PHS spectrum in the Gravel algorithm, to unfold the gamma ray and fast electron spectra from measurements collected in flight at different altitudes and latitudes.

The simulated results show approximate convergence with the results obtained using the EXPACS tool, for most altitudes and latitudes.

2. Setup on board the test aircraft

Figure 2 shows an image of the plastic scintillator that has been used during this measurement campaign and was manufactured by Eljen Technology. This scintillator is deployed to separately measure the raw energy spectra of gamma rays and neutrons, with a fast response time that allows the appropriate electronic system to record the signal generated by these two types of particles. The choice of this detector is also dictated by its good characteristics and its ability to efficiently detect and measure fast neutrons, due to the abundance of hydrogen in the consistency of the scintillating material shown in Table 1.

Vol. 6, No. 06; 2021

ISSN: 2456-3676

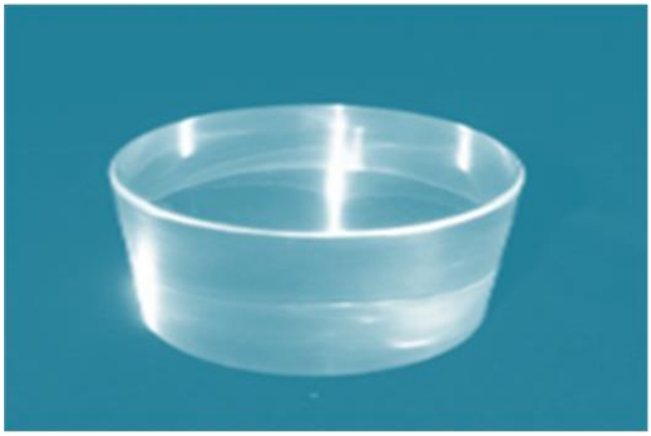

Figure 2. Plastic scintillator EJ 299-33A [16]

Table 1: Scintillator proprieties [16]

Proprieties	Scintillator
Output Light (% anthracene)	56
Scintillation efficiency	8600 photons/1MeVee
Wavelength of maximum emission (nm)	420
H Atoms per cm^3 (10^{+22})	5.13
C Atoms per cm^3 (10^{+22})	4.86
E Atoms per cm^3 (10^{+23})	3.55
Density (g/cm^3)	1.08

An ADIT B51 D01 (2” diameter and 10 stages) has been used as a photomultiplier (PMT), which contains a semi-transparent photocathode made of Bialkali materials, and having a maximum quantum efficiency of 25%.

The role of the dynodes installed inside the tube of this PMT is to multiply the number of photoelectrons generated by the recoil protons for the neutrons. On the other hand, the photoelectrons which are generated by the recoil electrons are allocated by the gamma rays, and this above-mentioned multiplication is carried out in order to obtain a sufficient signal current to be able to read it from a suitable electronic system. This is connected to the anode of the PMT via a preamplifier, whose role is to integrate the analog signal and then transmit it to the analog-to-digital conversion (ADC) system as shown in Figure 3. The first step of this process is the selection of the pulse samples needed to automatically create the statistical models to be used for the next step. The second step is to separate the pulse shapes, based on the decay time of the two light pulses generated by neutrons and gamma rays. The last step deals with the resulting pulses

Vol. 6, No. 06; 2021

ISSN: 2456-3676

which are then stored and displayed on the laptop by the corresponding energy of neutrons and gamma rays separately.

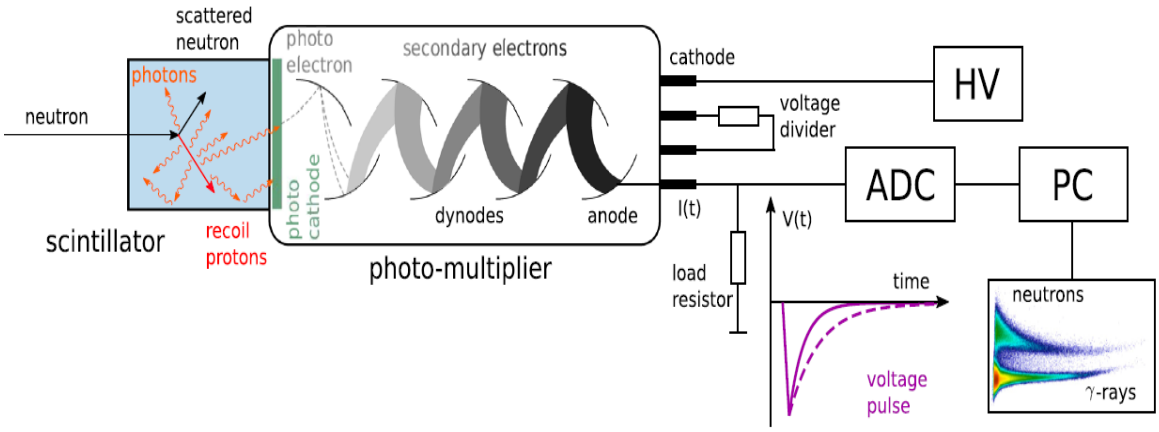

Figure 3. Typical setup using scintillator with PMT and ADC process [17]

The plastic scintillator and the PMT are surrounded by mu-metal that is a ferromagnetic material to protect the detector from external magnetic field that could affect the functionality of the PMT. In addition, the PMT and the scintillator interface are connected by optical grease, to improve the light collecting efficiency of the PMT. The entire detector is encased inside aluminum housing as shown in Figure 4.

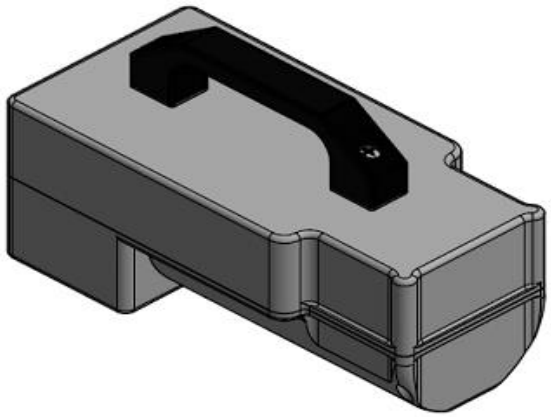

Figure 4. Detector enclosure

The conversion of the raw ADC channels into light energy in mega electron volt electron equivalent (MeVee), had been carried out, by using the calibration factors. This calibration is performed in the laboratory.

Vol. 6, No. 06; 2021

ISSN: 2456-3676

3. Assessment of gamma rays and electrons spectrums

3.1 Determination of the response function

The electromagnetic wave released by the gamma rays enters the detector, when it strikes any material, induced by the uncharged aspect of this particle. However, the incident electron does not penetrate into the material and only interacts with the surface of the detector window, due to the Colombian forces which this constantly undergo the loss of energy in the incident electron's track. In contrast, the interaction of gamma rays with scintillator material occurs mainly by Compton scattering, since the atomic number and density of a plastic scintillator are lower. Thus, other interactions with matter, such as photoelectric and pair production, are negligible in the plastic scintillator.

After the Compton scattering interaction has occurred, a scattered photon appears with a different trajectory than the initial trajectory and a recoil electron is then generated but with less energy than the incident gamma ray. The resulting recoil electron and the incident electron together interact with the molecules of matter in the same way, causing ionization and excitation along the path of electrons within the scintillator matter.

Since the radiative losses are insignificant in the plastic scintillator compared to those of the losses by collision. And even for the incident electrons at high energies, because of the low atomic number which characterizes the plastic scintillator [18]. Thus, the aforementioned excitation and ionization within the molecules of the scintillator material lead to optical photon emissions and therefore the resulting signal charges are then displayed in the installed electronic system. These pulses are proportional to the energies deposited by the two types of electrons mentioned above. Nevertheless, the relation between the spectrum of the pulse height (PHS) recorded at the installation as well as the energy spectrum of the gamma rays + incident electrons is given by the Fredholm integral of the first type, defined in the equation (1) [14, 19].

$$\frac{dN}{dH} = \int_0^{Emax} R\,(H,E)\phi(E)dE \qquad (1)$$

$\frac{dN}{dH}$: Differential pulse height spectrum measured;

R (H, E): Scintillator energy response functions;

(E): Gamma rays and electrons energies.

The above equation can be converted to the discrete form expressed in equation (2), since the PHS is collected from the multi-channel analyzer as deployed in the experimental platform used in this study.

Vol. 6, No. 06; 2021

ISSN: 2456-3676

(2)

$$N(H)_i = \sum_{J=1}^{m} R\ (H,E)_{ij}\phi(E)_j$$

Deducing the spectra of gamma rays and incident electrons from the collected PHS using the above equation is an ill-conditioned problem. This problem indeed requires solving the inverse equation by using mathematical algorithms, and for that, it is imperative to determine the energy response function R (H, E) ij of this plastic scintillator EJ299-33A. The dimensions of this response function are: i = number of channels and j = number of particle energy intervals. This matrix reflects the probability density function of the incident photon or electron at energy Ej, which is responsible for recording Hi, in the channel of the measuring system [11, 19]. Two methodologies are available for the determination of this response function: by the use of an appropriate experimental platform or, by the use of software based on the Monte Carlo method. This last alternative makes it possible to simulate the mode of interaction and the penetration trajectory of several types of incident particles in the absorbent material such as the plastic scintillator, for a multitude of energy values of this particle. However, the experimental method can determine the response function for a handful of energy values. This is due to the complexity of producing an assembly necessary to ensure the emission of mono-energetic photons from sources recognized worldwide in this kind of experience. Conversely, this method displays response function values close to what is actually displayed. Because in software using the Monte Carlo method, the simulated response function requires, in addition to performing a normalization, in order to make this simulated response coincide with that determined experimentally. Due to the omission to introduce certain parameters first in the code based on the Monte Carlo technique

In the present study, we have used the MCNP6 software to simulate the response function of the plastic scintillator installed on board the flight test aircraft for the measurement of gamma rays and atmospheric electrons. MCNP6 has been developed by the Los Alamos National Laboratory located in New Mexico, United States, since the 1940s. This software allows the simulation of the mode of interaction and the transport of this incident particle in the absorbent material [13]. To define the type of interactions that occur between the incident particle and the scintillating matter, the MCNP6 uses statistical models and sampling methods, based on random selection and deploying the laws of probability.

In addition, in MCNP6, the types of interactions that occur between the incident particles and the absorbent material are characterized by the values of the cross sections. These latter values are available and extracted from the evaluated nuclear data file (ENDF), which is integrated into the MNCP6 data. The value of the cross section is defined as the probability that the designed particle interacts with the defined matter for each type of interaction. Moreover, the geometric characteristics of the entire setup installed on board the airplane and the source characteristics are also included in the input file.

Vol. 6, No. 06; 2021

ISSN: 2456-3676

The materials making up the installation are also characterized in the input file. The F8 and FT8 PHL (pulse height light) counters are deployed in MCNP6 to simulate the equal probability response function for gamma rays and electrons only for a few energies. Gaussian energy broadening (GEB) is a specific function that is added in the FT8 counter, to take into account the low resolution of the plastic scintillator, by expanding the peaks and thus, bringing the simulations closer to the real operations of the scintillator [9, 11-12, 15, 20-23]. An interpolation of the energy responses, already simulated in MCNP6, is coded on MATLAB, with a step equal to 0.0128 MeV to correspond to the energy spectrum recorded since the setup.

3.2 Gravel algorithm

The determination of the energy spectrum of the gamma rays and the electrons which deploy from the PHS collected on the plastic scintillator, requires the simulation of the function of the energy responses. Their evaluation will be carried out under environmental conditions similar to those of the experimental setup. But this determination also involves the use of an adequate unfolding algorithm. In this option, many mathematical algorithms have been developed like artificial neural networks, genetic algorithms and least squares algorithms. This last type of algorithms was mainly developed by the PTB (Physikalisch technische bundesanstalt), like the Gravel algorithm. This model is the improvement of the SAND-II code and it was developed in 2002 by M. Matzke. This model had already been tested to unfold the gamma ray spectrum and succeeded in obtaining good results [14, 19]. Its great advantage is to avoid negative values for the calculated energy spectrum. The principles of the Gravel algorithm are to adjust the initial values (for k=1) of the fluence and to calculate the weight as shown by equation (3).

$$W_{ij}^{(k)} = \frac{R_{ij}\phi_j^{(k)}}{\sum_{j'=1}^{m} R_{ij'i}\,\phi_{j'}^{(k)}} \left(\frac{N_i}{\sigma_i}\right)^2 \quad (3)$$

Rij: Response matrix;

Ni: Count of measurements in the ith channel of the digital system;

σi: Standard deviation of Ni measurements.

The new fluence values are shown in the equation below.

$$T_j^{(k+1)} = T_j^{(k)} \exp \frac{\sum_{i=1}^{n} W_{ij}^{(k)} \ln \frac{N_i}{\sum_{j'=1}^{m} \left(R_{ij'}\phi_{j'}^{(k)}\right)}}{\sum_{i=1}^{n} W_{ij}^{(k)}} \quad (4)$$

Vol. 6, No. 06; 2021

ISSN: 2456-3676

The stopping of the iterative process is obtained either after having reached the convergence between the simulated results and the measurement records, or by minimizing $\chi 2$, by degree of freedom given in equation (5) and by maximizing the number of iterations.

$$(\chi^2)^{(k)} = \frac{1}{m} \sum_{i=1}^{n} \frac{\{ N_i - \sum_{j=1}^{m} R_{ij} \phi_j{}^{(k)} \}^2}{\sigma_i{}^2} \quad (5)$$

4. Simulation results and discussions

4.1 Estimation of the response function

A few energetic values have been selected to determine the mono-energetic response functions in the MCNP6 software. Figures 5, 6 and 7 show the curves of these responses by range of energy values: low, medium and high. Since the scale of these responses depends on the range of values of these previously arrested energies. An equal probability is applied for electrons and gamma rays to simulate these functions for selected energies greater than 0.125 MeV and a unit probability assigned to photons for energies less than 0.125 MeV. This is due to the non-linearity of the low energy electron response as low as 0.125 MeV, and also because of the predominance of the backscattering phenomenon in the interaction of the low energy electron with the absorbent material of the scintillator despite its low atomic number. Thus, after a backscattering interaction has occurred, a wide angle deviation of the incident electron from its initial projection onto the scintillator is highly likely. Thus leading to the ejection of this electron from the active volume of the scintillator. Because of the equality of the mass of the incident electron with the orbital electron positioned in the scintillating matter and also because of the low energy of the incident electron [18].

In addition, in the use of a material attributed to the plastic scintillator, the ideal response function assigned to an incident electron shows an absorption peak at the full energy of that electron. However, the shape of the ideal response function attributed to an incident photon has a shape that follows the continuous Compton profile to the Compton edges. This represents the maximum energy response that the photon can transmit to the recoil electron in the scintillator material [24]. However, the resulting deviation mentioned above can lead to the ejection of the electron from the scintillator, and in fact contribute to distorting the profiles of the response functions as is observed in the three figures cited above or even carry errors on the records collected. In addition, other parameters affect the profiles of the response function, notably the detector wall effect and the low energy resolution of the plastic scintillator [25], which leads to the display of the profiles as plotted on the three figures. The photon and the incident electron being able to strike the wall of the detector, a ratio of the energy deposited by these two particles can then not be carried out inside the active volume of the scintillator, mainly for particles of high energies. In addition, the low energy resolution which characterizes the plastic scintillator

Vol. 6, No. 06; 2021

ISSN: 2456-3676

can also lead to errors in the recorded measurements, since the detector equipped with this scintillator has a low capacity to display different signals for the incident particles with energies of close values [26].

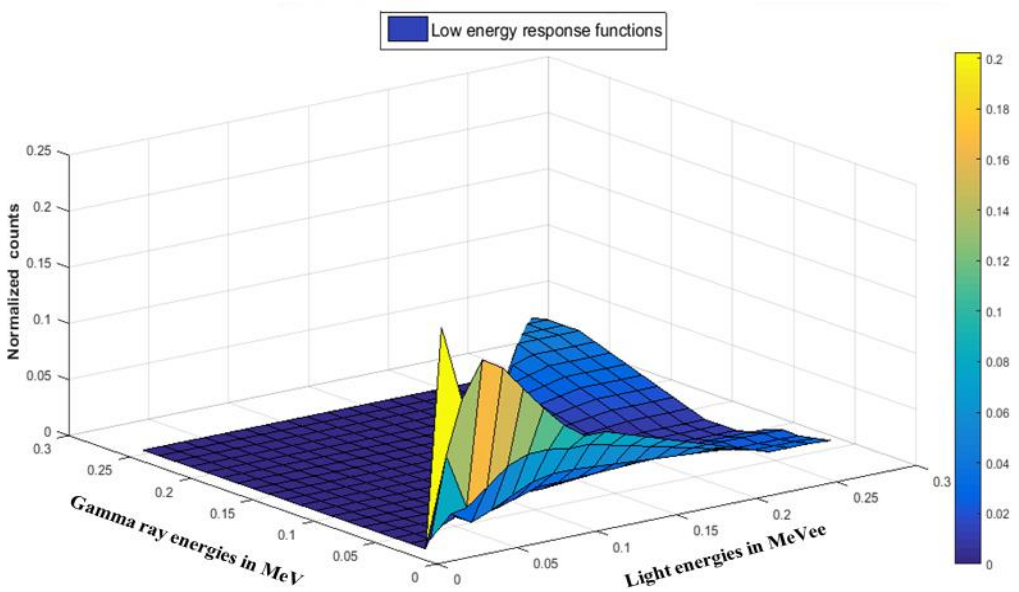

Figure 5. Low energy response functions

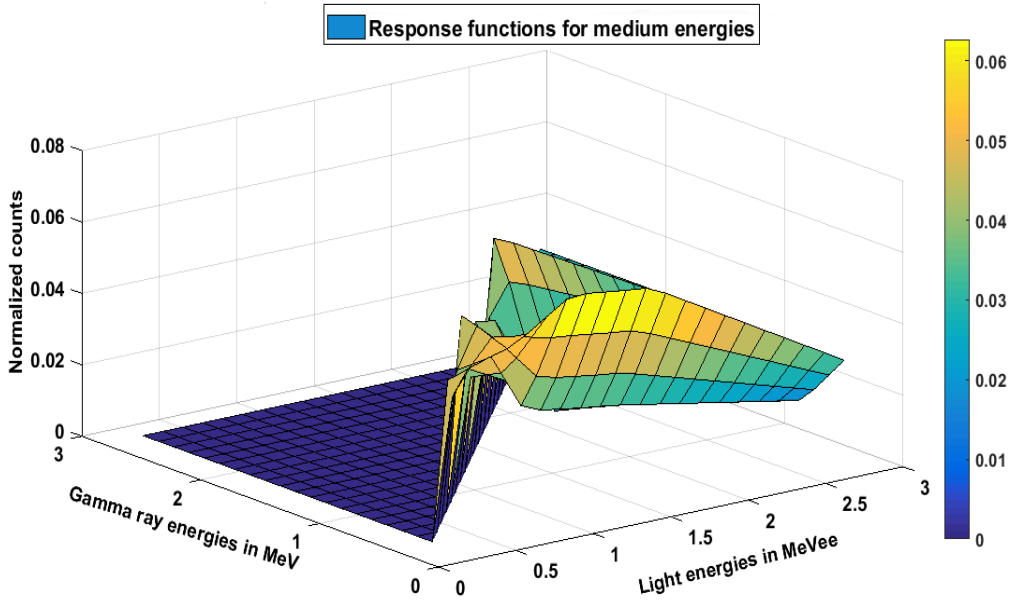

Figure 6. Response functions for medium energies

Vol. 6, No. 06; 2021

ISSN: 2456-3676

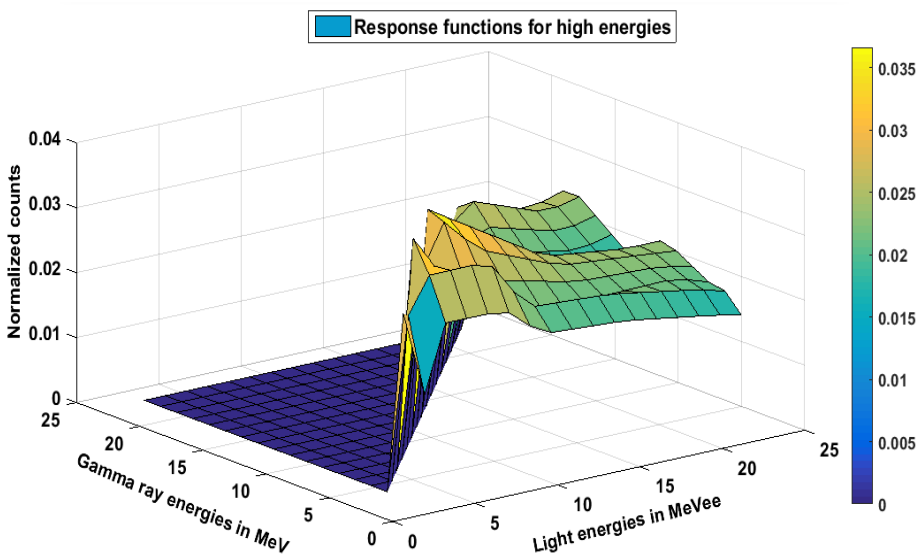

Figure 7. Response functions for high energies

4.2 Energetic spectrum by altitude

During each flight, the number of light pulses generated by the conversion of the energy deposited by cosmic particles into light is recorded in the electronic system installed on board the test aircraft. The discrimination between these particles is based on the difference in the decay time of the pulses generated by the energy deposited by the light particles in the form of electrons and the heavy particles in the form of protons. The first type of light pulses is mainly emitted at a fast time corresponding to fluorescence light, while the second type is mainly emitted at a longer time because it is influenced by phosphorescence light [11]. Thus, the amplitudes of the recorded light pulses are assigned to the channel numbers in the multi-channel analyzer installed in the electronic system [19].

Moreover, at each channel number of the multi-channel analyzer, a number of signals with the same amplitude are also collected every 10 seconds. This number represents the number of photoelectrons generated by each corresponding energy value that is deposited inside the active volume of the scintillator. Therefore, measurement spectra are collected with an energy step of 0.0128 MeVee and a synchronization step of 10 seconds. The first measurement spectrum corresponds to-the number of counts produced by the energies deposited jointly by the photons and the electrons, which are converted by scintillation into light energies of 0.0128 MeVee up to 25.4 MeVee. On the other hand, the second spectrum corresponds to the counts produced by the energies deposited by the incident neutrons. In this article, we have only studied the first spectrum of measurements mentioned above.

In addition, the experimental platform on board the test aircraft records for each flight every 10 seconds, longitude, latitude and altitude. These geographical coordinates correspond to the coordinates of the waypoints of the aircraft during the flight. And Table 2 provides the

Vol. 6, No. 06; 2021

ISSN: 2456-3676

geographic coordinates like longitudes, latitudes and altitudes of the seven flight path points selected from the measurement database to build this article. However, the energy interval corresponds to the interval for collecting records from the installation on board the test aircraft.

Table 2: Data for the flying trajectory points

Number of the point	Altitude on (km)	Latitude	Longitude	Energetic interval on (MeV)
1	14.5	36.5°	-100.2°	0 to 25.4 MeV
2	12.5	37.1°	-98.6°	0 to 25.4 MeV
3	10.5	37.5°	-99.4°	0 to 25.4 MeV
4	8.5	37.7°	-99.1°	0 to 25.4 MeV
5	6.5	37.6°	-98.7°	0 to 25.4 MeV
6	4.5	37.8°	-97.6°	0 to 25.4 MeV
7	2.5	37.7°	-97.9°	0 to 25.4 MeV

Once the energy response function is simulated in MCNP6, an interpolation of this matrix function is carried out in MATLAB to make the dimensions of this matrix coincide with the dimensions of the energy vector whose numbers of light pulses are recorded in the experimental installation.

The unfolding model through the Gravel algorithm is used to convert the PHS of measurements into the energy spectrum of photons and electrons together. An iterative process is then launched until the convergence is obtained, and thus gives the final fluence values for the photons and the electrons, that is to say after the fixing of the initial fluence values for the first iteration.

For each point mentioned in Table 2, and for every 5 minutes of flight time, a simulation is performed in MATLAB, that is to say after programming the Gravel algorithm in this mathematical tool.

Figures 8 to 11 show the final spectra of gamma rays and electrons using the Gravel algorithm for certain flight points as given in Table 2. In addition, in order to verify the accuracy rate of these simulated spectra, a comparison of two doses absorbed by the crew on board the aircraft for a 5 minute flight was made. The first dose refers to that estimated from the dose determined by the EXPACS tool. However, the second dose refers to that estimated by using the final fluence vector resulting from the simulation and the coefficients for converting fluence into effective dose which are published by the international commission on radiation protection (ICRP) in its publication n° 113.

It is judicious to recall that the coefficients of conversion of fluence into effective dose deployed in this study are those attributed to isotropic geometry. Because this type of geometry integrates the approximate calculation of the effective doses generated by the exposure of this geometry to external radiation including all directional incidences such as exposure to atmospheric cosmic

Vol. 6, No. 06; 2021

ISSN: 2456-3676

radiation of the crew on board the airplane [13, 27]. These mono-energetic coefficients consist of converting the fluence into effective dose per energy value [27].

The data shown in Table 3, give, for each point of flight, the number of iterations necessary to obtain the convergence of the fluence spectrum of photons and electrons jointly in the Gravel algorithm. This table also gives the values of $\chi 2$ and the number of iterations necessary to establish the convergence of this fluence vector. Finally, the same table presents the relative error between the effective doses obtained from the measurements and those estimated by EXPACS. Figures 8 to 11 show the final spectra for flight points n° 1, n° 2, n° 4 and n° 6 respectively as given in Table n° 2.

Table 3: Simulation results

Point number	Number of the iteration	Chi-square χ^2	Effective dose from EXPACS on (pSv)	Effective dose from unfolding measurements spectrum on (pSv)	Relative difference between the two doses on (%)
1	59	0.85	$4.5\ 10^4$	$3.6\ 10^4$	19.5
2	69	0.86	$3.7\ 10^4$	$3.1\ 10^4$	17.3
3	75	0.86	$2.5\ 10^4$	$2.1\ 10^4$	14.0
4	77	0.58	$1.4\ 10^4$	$1.2\ 10^4$	18.6
5	40	0.39	$6.3\ 10^3$	$7.5\ 10^3$	15.8
6	80	0.37	$2.1\ 10^3$	$3.1\ 10^3$	31.7
7	110	0.36	$1.4\ 10^3$	$2.3\ 10^3$	38.65

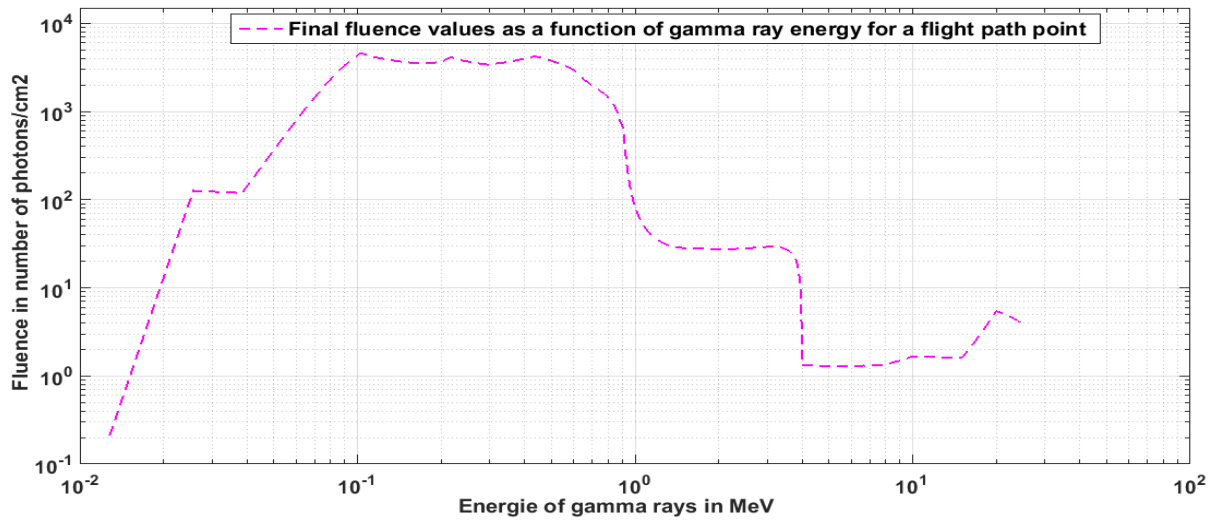

Figure 8. Fluence spectrum of gamma rays at point n° 1

Vol. 6, No. 06; 2021

ISSN: 2456-3676

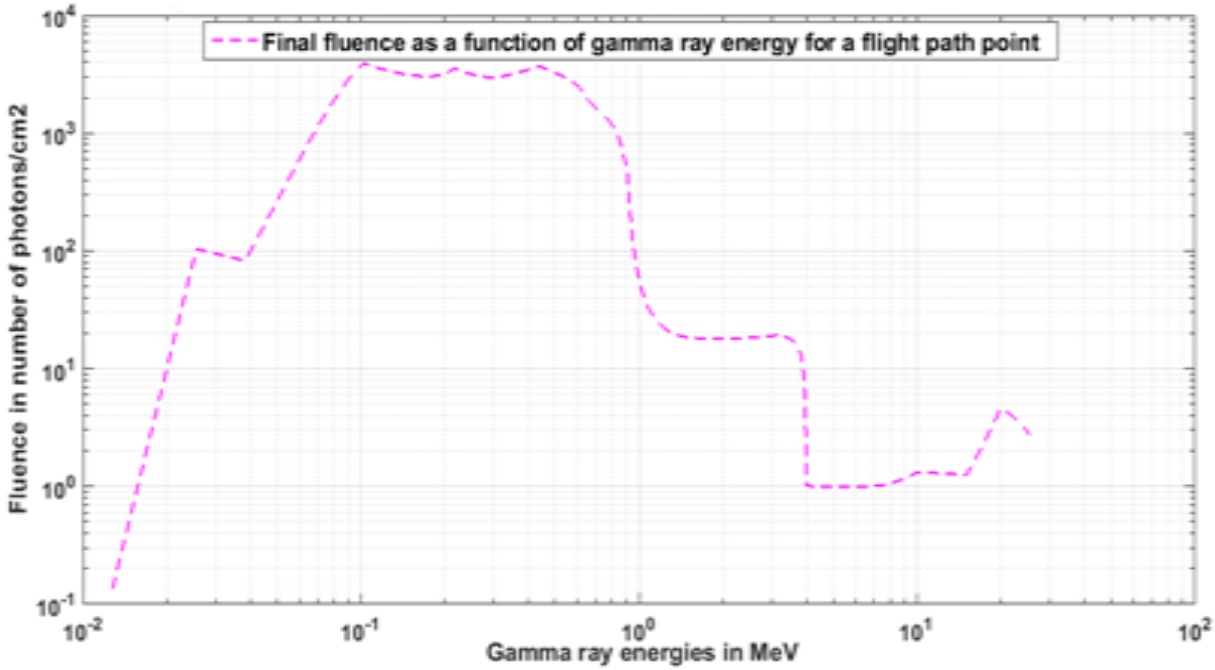

Figure 9. Fluence spectrum of gamma rays at point n° 2

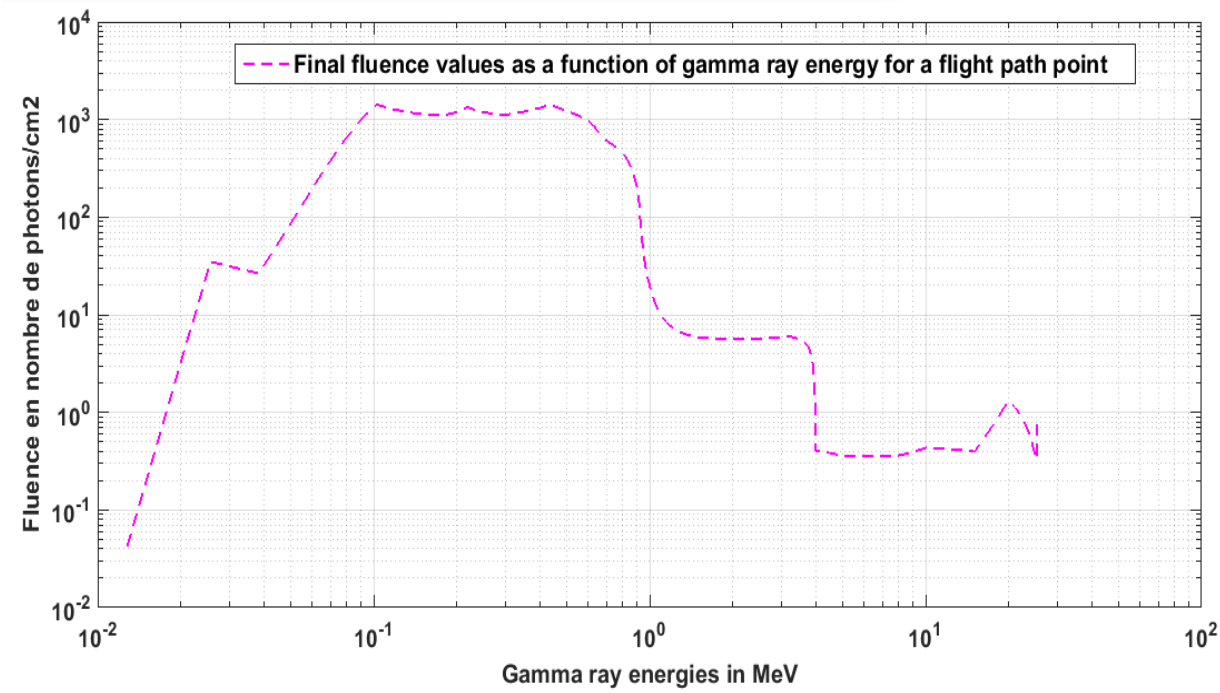

Figure 10. Fluence spectrum of gamma rays at point n° 4

Vol. 6, No. 06; 2021

ISSN: 2456-3676

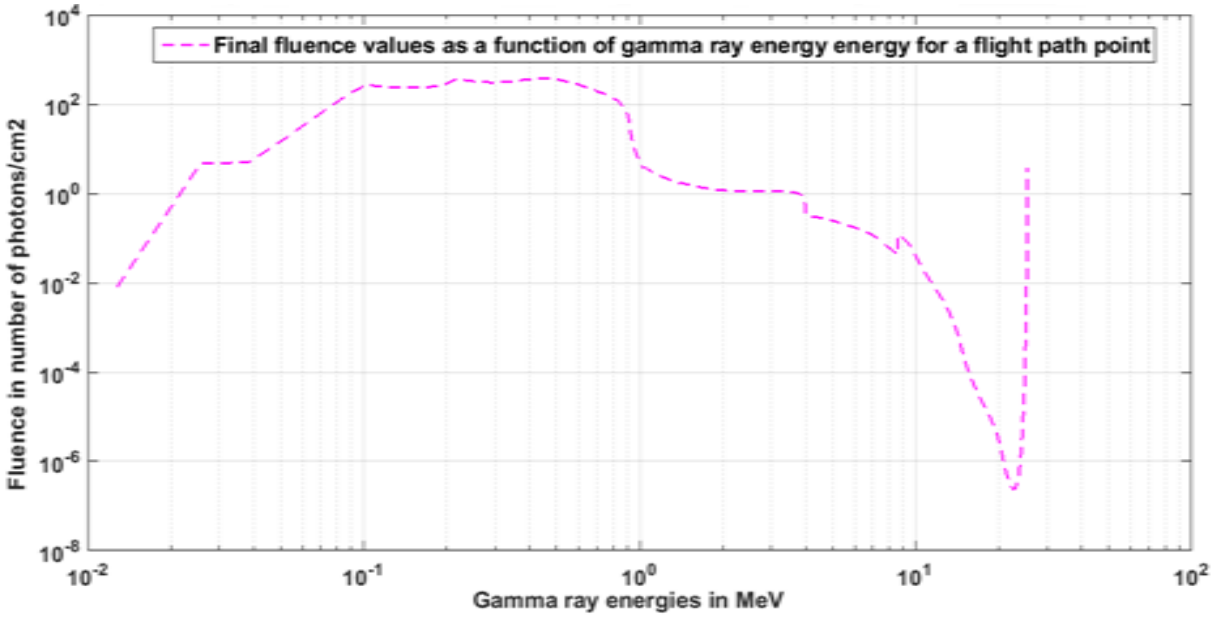

Figure 11. Fluence spectrum of gamma rays at point n° 6

The profiles of the response functions simulated in MCNP6 have been distorted by many parameters because none of the full energy peaks and Compton edges is reached at adequate energy. The wall effect is one of these deforming effects, since this parameter is redoubtable for photons and electrons with high energy, especially in small to medium active areas such as the scintillator used in this study [11]. This effect can also distort the measurements collected from the experimental installation on board the aircraft for high energy particles. To this end, this parameter can lead to divergences in the fluence values at high energies as observed on curves n° 10 and n° 11 and can particularly cause significant differences between the two effective dose values as seen in points of flight n° 6 and n° 7. Because, the fluence values at high energy are overestimated as can be seen mainly in curve n° 11, which leads to the overestimation of the effective doses at these energy values.

On the other hand, it is observed that the divergences are anti-proportional to the values of the altitudes, probably due to the increase in the fluence spectrum at high energies for high altitudes compared to the fluence spectra displayed at low altitudes. This makes these deviations more important for the low altitudes compared to the high altitudes. Moreover, in chapters 3 and 4 of this article, it was indicated that an interpolation was carried out in order to have similar dimensions between the response matrix and the vector of the collected measurements. Therefore, this huge interpolation can also lead to deviations in the fluence spectra mainly at the end of the process which is long and rich in intermediate steps.

In addition, although the bremsstrahlung interaction has a low probability in the plastic scintillator, the distortion in the PHS that it generates is therefore very low. However, the distortions caused by the backscattering phenomenon are quite important on the response

Vol. 6, No. 06; 2021

ISSN: 2456-3676

functions, especially at low energies and can even cause errors in the measurements recorded at low energy electrons [18]. Therefore, all of these errors can lead to the discrepancies and differences in results mentioned above.

5. Conclusion

To perform better detection and measurement of gamma rays and electrons simultaneously, by using only one type of detector, a delicate compromise is required between the thickness and the atomic number of the material constituting this detector. A large thickness and a high atomic number are favourable to the detection of penetrating gamma rays. However, low thickness and low atomic number are advantageous for detecting fast electrons, in order to avoid or reduce backscattering and bremsstrahlung phenomena. In addition, the unfolding of the measured spectra may ignore the backscattering phenomenon, since the response functions having been simulated, may not take this phenomenon into account in the simulation process. Unlike, measured spectra which reflect real data and therefore cannot ignore this phenomenon [18]. It is probably for this reason that the effective doses deduced from the Gravel algorithm are always higher than the doses calculated from the EXPACS tool. But overall, the results are consistent, despite the spectral divergences for energies above 20 MeV recorded mainly for low altitudes. In addition, the size of the detector plays a proportional role in reducing the wall effect, which allows the particle to deposit all of its energy inside the active volume of the detector. Moreover, the size of the plastic scintillator used in this study is small to medium, so the impact of the wall effect is not overlooked.

Moreover, according to the results and conclusions presented above, the plastic scintillator has relatively the capacities of detecting the various particles of cosmic radiation at the flight altitudes of airplanes. Although this scintillator does not have good energy resolution and has a low atomic number. On the other hand, this type of detector has good temporal resolution and the ability to discriminate between particles in the mixed radiation field. In addition, the plastic scintillator has a high efficiency in the detection of fast neutrons, which is the study that will follow this article. The study of neutron quantification will be undertaken soon, because neutrons present a real risk on on-board systems. This is due to the potential possessed by atmospheric neutrons to trigger a SEU on the electronic systems installed on board the aircraft [28-29].

Acknowledgments

The authors would like to thank the management of Bombardier Aerospace, without whom this project never saw the light of day, and who also made it possible to undertake the radiation measurement campaign on board a test aircraft. We must remind and thank here the technical support of our partners and their contribution to the data collection devices, as well as their dedicated software installed on board the test aircraft.

Finally, funding for this research activity was provided by CARIC/CRIAQ, as well as by Mitacs which initiated the grant [AVIO 1603].

Vol. 6, No. 06; 2021

ISSN: 2456-3676

References

Edwards R., Dyer C. and Normand E. 2004. "Technical Standard for Atmospheric radiation event effect (SEE) on avionics electronics." IEEE Conf. on Radiation effects Data workshop: 1-5. DOI: 10.1109/REDW.2004.1352895.

Office for Official Publications of the European Communities. 2004. "Cosmic Radiation Exposure of Aircraft Crew: Compilation of Measured and Calculated Data." 281p. ISBN 92-894-8448-9.

Durante M. and Cucinotta F. A. 2011. "Physical basis of radiation protection in space travel." Reviews of Modern Physics, 83:1245-78

Vainio R., Desorgher L., Heynderickx D., Storini M., Flückiger E., Horne R.B., Kovaltsov G.A., Kudela K., Laurenza M., McKenna-Lawlor S., Rothkaehl H. and Usoskin I.G. 2009. "Dynamics of the Earth's Particle Radiation Environment." Space Science Reviews, 147:187-231. DOI: 10.1007/s11214-009-9496-7

Aerospace. 2012. "Development of Atmospheric Neutron Single Event Affects Analysis for use in Safety Assessments." Report. AIR 6219.31p

Letessier-Selvon A. and Stannev T. 2011. "Ultrahigh Energy Cosmic Rays Reviews of Moden Physics." Review of Modern Physics, 83(3): 1- 40. DOI: 10.1103/RevModPhys.83.907

Preston R. M., Eberhardt J. and Tickne J. 2014. "Neutron-gamma pulse shape discrimination using organic scintillators with silicon photomultiplier readout." IEEE Transactions on Nuclear Science, 61(4): 2410-2418. DOI: 10.1109/TNS.2014.2335208

Hamel M. and Carrel F. 2017. "Pseudo-gamma spectrometry in plastic scintillators in New Insights on Gamma Rays ed A M Maghraby (Rigeka)." 20p

Orion I. 2019. "Gamma radiation measurements in Advances in Radiometry ed Avidscience (Telangana)." 31p

Nakamura T. 2003. "Recent Development of Advanced Neutron Detection Technology." Journal of Nuclear and Radiochemical Sciences, 4(2): R15-R24

Knoll G.F. 2000."Radiation Detection and Measurement." 3rd Edition. John Wiley & Sons, Inc. 802p. ISBN 0-471-07338-5

Quin J., Lai C., Lu X., Zheng P., Zhu T., Liu R., Ye B. and Zhan X. 2018. "Characterization of a 6Li enriched Cs2LiYCl6:Ce scintillator and its application as a γ-ray detector." Nuclear Instruments & Methods in Physics Research Sectio A, 886:55-60. DOI: 10.1016/j.nima.2017.11.053

Van Rooyen T. J. 2015. "Transport and Shielding of Ionising Radiation (Manual. South African Nuclear Energy Corporation)." 533p

Matzke M. 1997. "Unfolding of Particle Spectra. International Conference: Neutrons in Research and Industry," Proceedings of SPIE, 2867:598-607. DOI: 10.1117/12.267860

Vol. 6, No. 06; 2021

ISSN: 2456-3676

Mouhti I., Elanique A. and Messou M. Y. 2017. "Monte Carlo Modeling of NaI (TI) scintillator detectors using MCNP simulation code." Journal of Material and Environmental Sciences,8(12): 4560-65. DOI: 10.26872/jmes.2017.8.12.481

https://eljentechnology.com/products/plastic-scintillators/ej-276

Cecconello M. 2019. "Liquid Scintillators Neutron Response Function: A Tutorial." Journal of Fusion Energy, 38: 356-75. DOI: 10.1007/s10894-019-00212

Tsoulfanidis N.1995. "Measurement and Detection of Radiation." 2nd Edition. Taylor and Francis. 614p. ISBN10 1560323175

Chen Y., An L., Chen X. and Jianxiong W. 2014. "Unfolding the fast Neutron Spectra of BC 501A liquid Scintillation detector using Gravel method." Science China physics Mechanics and Astronomy, 571(10): 1885-90, 2014. DOI: 10.1007/s11433-014-5553-7

Su-Ya-La-Tu Z., Zhi-Qiang C., Rui H., Xing-Quan L., Wada R., Wei-Ping L., Zeng-Xue J., Yin-Yin X., Jian-Li L. and Fu-Dong S. 2013. "Study on gamma response function of EJ301organic liquid scintillator with GEANT4 and FLUKA." Chinese Physics C, 7(12): 126003.1-6

Oak Ridge National Laboratory. 2014. "MCNP6 Users Manual - Code Version 6.1.1beta." Radiation Safety Information Computational. LA-CP-14-00745. Center «RSICC»

Hakimabad H. M., Panjeh H. and Vejdani-Noghreiyan A. 2007. "Function of 3X3in.NaI Scintillator Detector in the range of 0.081 to 4.738 MeV." Asian Journal of Experimental Sciences, 2 (2): 233-37

Li X., Wang Y., Zhou R. and Yan C. 2017. "Energy calibration for plastic scintillation detectors based on Compton scatterings of gamma rays." Journal of Instrumentation, 12(12): 1-11

Jianguo Q., Lai C., Ye B., Liu R., Zhang X. and Jiang L. 2015. "Characterizations of BC 501A and BC 537 Liquid scintillators detectors." Radiation and Isotopes, 104: 15-24

Shin K. 1979. "Calculation of Response Function of NE-213 Organic Liquid Scintillator for Gamma-Rays." Journal of Nuclear Science and Technology, 6(6): 390-400

Holland H.D. and Turekian K.K. 2014. "Treatise on Geochemistry." 2nd Edition (Volume 1-16). Elsevier Science. 9144p. ISBN: 9780080983004

ICRP. 2010. "Conversion Coefficients for Radiological Protection Quantities for External Radiation Exposures ICRP Publication 116," Ann. ICRP40 (2–5)'. 257p

Taber A. and Normand E. 1993. "Single event upset in avionics." IEEE Transcations on Nuclear Science, 40(02): 120-26. DOI: 10.1109/23.212327

Normand E. 1996. "Single event effects in Avionic." IEEE Transactions on Nuclear Science, 43(02): 461-73. DOI: 10.1109/23.490893